Medical Oncology (2025) 42:123
https://doi.org/10.1007/s12032-025-02662-z

ORIGINAL PAPER

Integrative analysis of ubiquitination-related genes identifies HSPA1A as a critical regulator in colorectal cancer progression

Xinji Gao[1] · Ting Yan[1] · Xiang Yu[1] · Qiang Li[1] · Lan Zhao[1] · QingShui Wang[2] · Jun Wang[1]

Received: 7 January 2025 / Accepted: 4 March 2025 / Published online: 20 March 2025

Abstract

Colorectal cancer (CRC) is a prevalent and lethal malignancy, with ubiquitination significantly influencing cellular processes involved in cancer progression. However, the contributions of ubiquitination-related genes in CRC remain unclear. This study conducted a detailed analysis of gene expression profiles associated with ubiquitination in CRC, evaluating 1006 genes across 46 pathways. By comparing CRC tissues to adjacent normal tissues, we identified differentially expressed genes and developed a ubiquitination-related pathway gene signature (URPGS) using LASSO regression analysis on genes with prognostic significance. The prognostic capability of the URPGS was validated in independent cohorts, and its associations with clinical characteristics, including post-chemotherapy survival outcomes, were examined. Machine learning techniques identified HSPA1A as a key gene relevant to CRC both in vitro and in vivo. Our analysis revealed 307 differentially expressed ubiquitination-related genes, with 24 significantly associated with patient prognosis. The developed 14-gene URPGS exhibited strong prognostic value, effectively stratifying patients into high-risk and low-risk groups for overall survival. The URPGS correlated with advanced clinical stages, lymph node metastasis, and recurrence, with higher scores linked to poorer post-chemotherapy survival outcomes. Knockdown of HSPA1A significantly inhibited CRC cell proliferation, migration, and invasion in vitro, as well as tumor growth and metastasis in vivo. This research establishes a novel URPGS that effectively predicts prognosis and chemotherapy outcomes in CRC, enhancing our understanding of ubiquitination's role and suggesting personalized treatment strategies.

Keywords Colorectal cancer · Ubiquitination · Biomarker · Prognosis · HSPA1A

Introduction

Colorectal cancer (CRC) stands as one of the most widespread and deadly cancers globally, posing significant challenges to public health [1–3]. Despite advancements in diagnostic techniques and therapeutic strategies, the prognosis remains grim for many CRC patients, especially those with advanced-stage disease [4, 5]. This highlights an urgent need for new biomarkers and therapeutic targets to enhance patient outcomes.

In recent years, there has been growing interest in the role of post-translational modifications, especially ubiquitination, in cancer development. Ubiquitination involves the covalent attachment of ubiquitin molecules to target proteins, influencing their stability, localization, and function. This process is regulated by a cascade of enzymes, including E1 activating enzymes, E2 conjugating enzymes, and E3 ligases, while deubiquitinating enzymes counteract this by removing ubiquitin chains. The ubiquitination pathway is crucial for cellular functions such as protein degradation, DNA repair, and signal transduction. Dysregulation of this pathway has been linked to various diseases, particularly cancer. In CRC, abnormal ubiquitination affects key oncogenes and tumor suppressors, contributing to tumor initiation, progression, and metastasis.

Xinji Gao and Ting Yan have contributed equally to this work.

✉ QingShui Wang
wangqingshui@fjtcm.edu.cn; wangqingshui@fjnu.edu.cn

✉ Jun Wang
1095077121@qq.com

[1] The Second Affiliated Hospital of Fujian University of Traditional Chinese Medicine, Fuzhou, China

[2] Fujian-Macao Science and Technology Cooperation Base of Traditional Chinese Medicine-Oriented Chronic Disease Prevention and Treatment, Innovation and Transformation Center, Fujian University of Traditional Chinese Medicine, Fuzhou, China

In this study, we perform a comprehensive analysis of ubiquitination-related gene expression profiles in CRC. Our objectives include identifying differentially expressed genes between CRC tissues and adjacent normal tissues and developing a ubiquitination-related pathway gene signature (URPGS) for prognostic prediction. By incorporating machine learning approaches, we identified HSPA1A as a key gene within the URPGS, which may serve as a biomarker or therapeutic target. HSPA1A is a molecular chaperone that assists in protein folding and promotes the degradation of misfolded proteins, preventing toxic accumulation in cells. We also plan to validate the functional significance of HSPA1A through in vitro and in vivo experiments. This approach enhances our understanding of ubiquitination-related genes in CRC and lays the foundation for novel prognostic tools and therapeutic strategies, ultimately improving patient outcomes.

Methods

Data acquisition

Data for the GSE17536 [6] and GSE87211 [7] cohorts were sourced from the GEO database. Microarray data were normalized and preprocessed using the Robust Multi-array Average (RMA) method with the Affy package in R [8]. Colorectal cancer gene expression data, quantified as fragments per kilobase million (FPKM), along with relevant clinical details, were collected from The Cancer Genome Atlas (TCGA) through the sangerbox platform (http://vip.sangerbox.com/home.html). The FPKM values were converted to transcripts per kilobase million (TPM) for subsequent analyses. The GSE17536 cohort includes 177 colorectal cancer patients with follow-up data, while the GSE87211 cohort comprises 203 colorectal cancer samples and 160 mucosa control samples. TCGA provides data for 459 colorectal cancer patients.

Identification of ubiquitination-related pathway gene

We identified ubiquitination-related pathway gene by querying the term" ubiquitination" in the Molecular Signatures Database (MSigDB). This search yielded 1,006 genes across 46 ubiquitination-related pathways, as detailed in Supplementary Table 1.

Differential gene expression analysis

The expression profiles of ubiquitination-related pathway genes in colorectal cancer and adjacent normal tissues were analyzed using the "limma" package in R. Genes were considered differentially expressed and selected for further analysis based on criteria of |log2 fold change (FC)|≥ 0.585 and a p-value < 0.05.

Functional enrichment analysis

To explore the potential biological processes and pathways associated with these differentially expressed genes, KEGG and Gene Ontology Biological Process (GO-BP) enrichment analyses were performed. A threshold of adjusted p-value < 0.05 was set to determine significant pathways or processes.

Construction of a URPGS for colorectal cancer

To determine ubiquitination-related pathway genes with prognostic value, a univariate Cox regression analysis was executed using data from the TCGA cohort. Genes with a p-value < 0.05 underwent further selection through the Least Absolute Shrinkage and Selection Operator (LASSO) Cox regression analysis. LASSO employs L1 regularization to drive the coefficients of less relevant features to zero during fitting. Only features with non-zero coefficients were retained in the model, as those with zero coefficients were considered non-essential. The genes retaining non-zero coefficients were identified as the final prognostic genes, forming the basis for constructing the URPGS model: (coefficient of gene 1 × expression of gene 1) + (coefficient of gene 2 × expression of gene 2) + ⋯ + (coefficient of gene n × expression of gene n).

Immune infiltration analysis

To assess immune infiltration in colorectal cancer, we utilized ESTIMATE, CIBERSORT, and XCELL algorithms. The relationship between the URPGS and various immune cell populations was examined.

Single-cell level analysis

The Tumor Immune Single-cell Hub 2 (TISCH2) [9], referred to as the Tumor Immune System Atlas, is a scRNA-seq database concentrating on the tumor microenvironment (TME). This resource provides comprehensive cell-type annotations at the single-cell level, facilitating in-depth examination of the TME across a range of cancer types.

Machine learning model

For classifying data samples, we employed several machine learning models including XXGBoost, Logistic Regression, LightGBM, Random Forest, AdaBoost, Decision Tree, GBDT, Gaussian Naive Bayes (GNB), and Complement

Naive Bayes (CNB) via the Extreme Smart Analysis platform (https://www.xsmartanalysis.com/). Each model underwent meticulous parameter tuning and optimization, utilizing cross-validation for validation purposes. Specifically, we set the random seed to 41 and used a twofold cross-validation approach. The test set comprised 15% of the total data samples. The performance of each model was assessed using ROC curves and a variety of other performance metrics.

Nomogram construction

A nomogram was developed using the rms package. To assess its predictive performance, a confusion matrix and the area under the receiver operating characteristic (ROC) curve (AUC) were utilized. The effectiveness of the nomogram was further validated by applying a bootstrapping validation with 1,000 bootstrap resamples.

Cell cultivation

Colorectal cancer cell lines HCT-116 and DLD1, sourced from the American Type Culture Collection (ATCC), were utilized in this study. These cells were propagated in Dulbecco's Modified Eagle Medium (DMEM) supplemented with 10% fetal bovine serum (FBS) and 1% penicillin–streptomycin. Cultivation was carried out at 37 °C in a humidified atmosphere containing 5% CO_2. All cell lines were authenticated by short tandem repeat profiling (2023.06).

Quantitative real-time PCR (qRT-PCR)

Cells were processed to extract total RNA using TRIzol reagent (Invitrogen), followed by reverse transcription into cDNA via the PrimeScript RT reagent Kit (TaKaRa, Japan). QRT-PCR analysis was conducted using SYBR Premix Ex Taq (TaKaRa), with GAPDH serving as the internal reference. Relative mRNA expression levels were determined through the $2^{-\Delta\Delta CT}$ approach. The primers utilized for amplifying HSPA1A were: forward 5′-AGCTGGAGCAGG TGTGTAAC-3′ and reverse 5′-CAGCAATCTTGGAAA GGCCC-3′. The primers for GAPDH included a forward sequence of 5′-GGTGAAGGTCGGAGTCAAC-3′ and a reverse sequence of 5′-CAAATGAGCCCCAGCCTTC-3′.

Cell proliferation assay

The proliferation of cells was evaluated using the Cell Counting Kit-8 (CCK-8) method. In short, cells were plated in 96-well plates at a concentration of 2×10^3 cells per well. At 0, 24, 48, and 72 h post-seeding, the CCK-8 solution was introduced to each well and incubated at 37 °C for 2 h. The absorbance was then read at 450 nm with a microplate reader.

Wound healing assay

Cells were cultured to confluence in 6-well plates, and a scratch was inflicted with a sterile 10-µL pipette tip. Following a PBS wash, the cells were incubated in a medium devoid of serum. Images were taken at the time of scratching and again at 48 h using an inverted microscope. The rate of wound closure was then assessed using ImageJ software.

Transwell invasion assay

The invasive capability of cells was assessed using Transwell chambers coated with Matrigel (Corning, NY, USA). In summary, 2×10^4 cells were plated in the upper chamber with a serum-free medium, and the lower chamber was filled with medium containing 10% FBS. After 24 h, cells that did not invade were cleared away, while the cells that had invaded were fixed, stained with crystal violet, and counted under a microscope.

Zebrafish xenograft model

The zebrafish xenograft model was established to evaluate the in vivo tumor growth and metastatic potential of HCT-116 colorectal cancer cells. Zebrafish (Danio rerio) were obtained from Fuzhou Bio-Service Biotechnology Co. Ltd (Fuzhou, China) and maintained under standard laboratory conditions at 28.5 °C with a 14:10-h light–dark cycle. For xenotransplantation, HCT-116 cells were first digested with trypsin and labeled with 5 µM 1,1′-dioctadecyl-3,3,3′,3′-tetramethylindocarbocyanine perchlorate (Dil; Meilun Biotechnology, China), a red fluorescent lipophilic membrane dye, to enable precise tracking of cell migration and proliferation. The xenotransplantation procedure was performed using GB100T-8P glass capillaries and FemtoJet 4i microinjectors (Eppendorf, Germany). Approximately 200 labeled HCT-116 cells were carefully injected into the central yolk sac or ventral yolk cavity of zebrafish larvae aged 2–3 days post-fertilization, with each experimental group consisting of ten larvae to ensure statistical reliability. Fluorescence microscopy was used to monitor tumor cell dynamics at two critical time points: for proliferation assessment, imaging was conducted at 2 h and 48 h post-transplantation (hpt) to evaluate initial cell distribution and tumor cell growth, respectively; for metastasis assessment, tail fluorescence was recorded at 2 h and 24 h post-transplantation (hpt) to analyze cell migration and metastatic potential. Experiments involving zebrafish larvae younger than 5 days do not require ethics committee approval. The study complied with ARRIVE guidelines for animal research reporting.

Statistical analysis

Experiments were conducted in triplicate, with data expressed as mean ± standard deviation (SD). Statistical evaluations were performed using GraphPad Prism version 8.0. Comparisons between two groups utilized Student's t-test, while one-way ANOVA was employed for analyses involving more than two groups. A p-value of less than 0.05 was considered indicative of statistical significance.

Results

Workflow of this study

In this study, we analyzed the differentially expressed ubiquitination-related pathways gene between in colorectal cancer based on TCGA cohort. Based on these genes, we developed a prognosis model for colorectal cancer. The detailed workflow of this research is depicted in Fig. 1.

Comprehensive analysis of ubiquitination-related pathways gene expression profiles in colorectal cancer

In order to thoroughly investigate the expression profiles of genes involved in ubiquitination-related pathways in colorectal cancer, we initially conducted an analysis assessing the expression levels of 1006 genes across 46 ubiquitination-related pathways in colorectal cancer tissues. Our findings revealed that, compared to adjacent normal tissues, 144 genes were significantly upregulated, while 163 genes were significantly downregulated in colorectal cancer tissues (Fig. 2A, B). To assess the discriminative power of these differentially expressed genes, we performed UMAP analysis, which demonstrated that these 307 genes effectively distinguished colorectal cancer tissues from adjacent normal tissues (Fig. 2C), highlighting their potential as biomarkers for colorectal cancer diagnosis.

To delve further into the biological significance of these differentially expressed genes, we conducted pathway enrichment analyses. KEGG pathway analysis indicated that upregulated genes were predominantly enriched in signaling pathways such as Cell Cycle, Pathways in Cancer, Ubiquitin-Mediated Proteolysis, and Progesterone-Mediated Oocyte Maturation (Fig. 2D). Similarly, Gene Ontology Biological Process (GO-BP) analysis showed

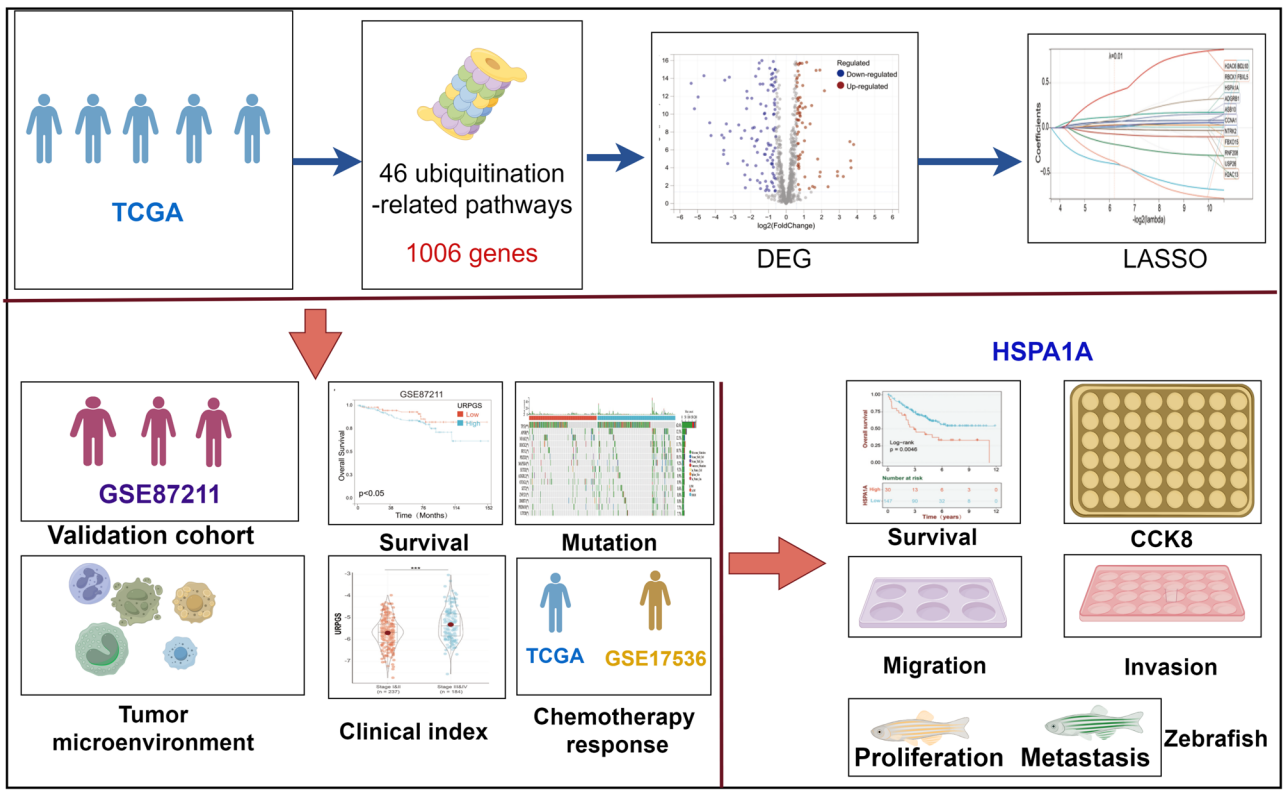

Fig. 1 Flowchart for comprehensive analysis of prognostic model based on ubiquitination-related pathway genes in colorectal cancer

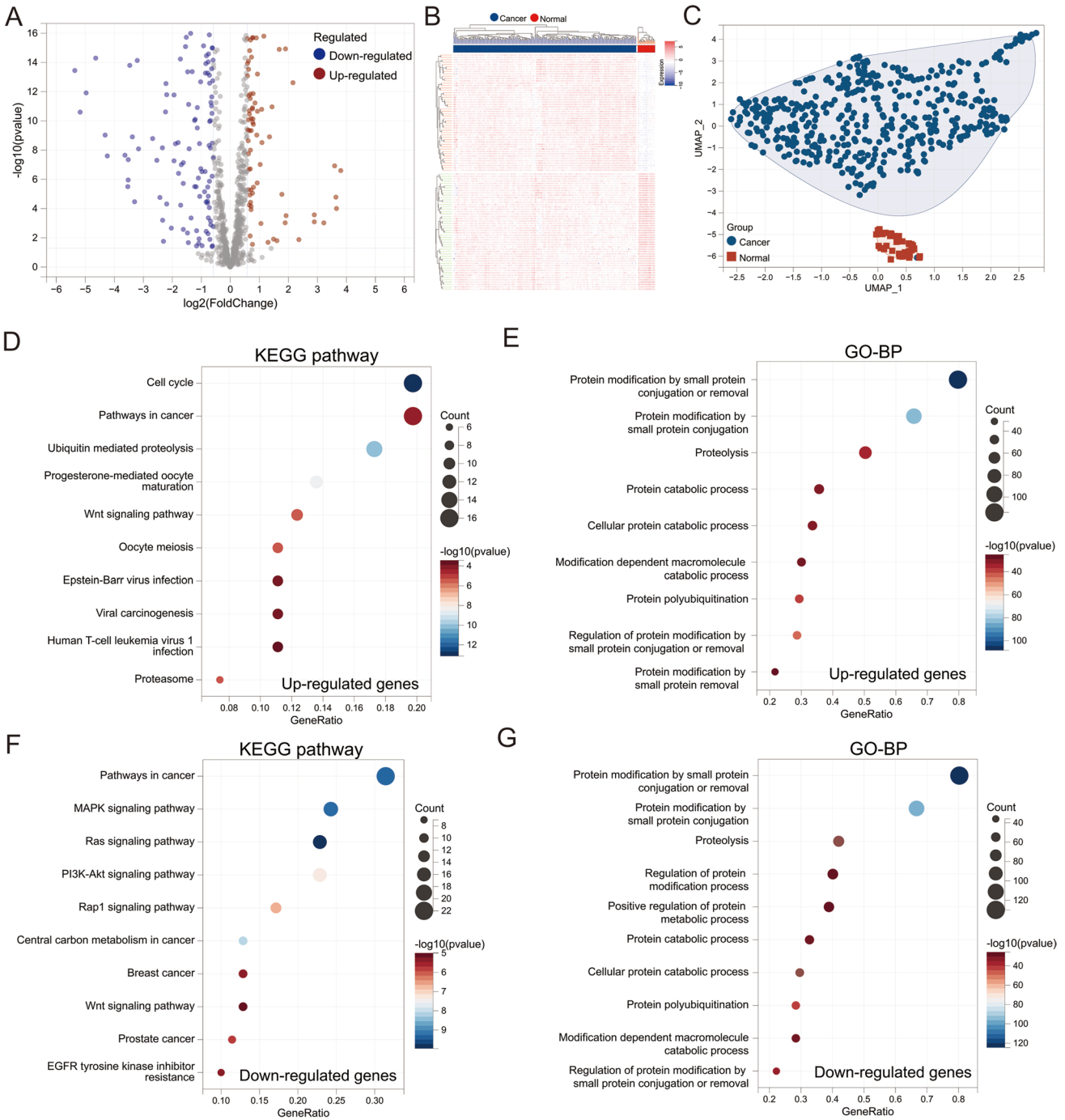

Fig. 2 Comprehensive analysis of ubiquitination-related pathway gene expression profiles in colorectal cancer. **A** Volcano plot and **B** heatmap illustrating the differentially expressed genes between colorectal cancer tissues and adjacent normal tissues. **C** UMAP analysis demonstrating the ability of 307 differentially expressed genes to distinguish colorectal cancer tissues from normal tissues. **D** and **E** Enrichment analyses for upregulated genes, with **D** highlighting the KEGG pathways and **E** detailing the GO-BP terms. **F** and **G** Enrichment analyses for downregulated genes, featuring **F** KEGG pathways and **G** GO-BP terms

significant associations with processes including Protein Modification by Small Protein Conjugation or Removal, Proteolysis, and Protein Catabolic Process (Fig. 2E). In contrast, KEGG pathway analysis of the 163 downregulated genes revealed enrichment in pathways such as Pathways in Cancer, MAPK Signaling Pathway, Ras Signaling Pathway, and PI3K-Akt Signaling Pathway (Fig. 2F). GO-BP analysis further indicated that these downregulated genes were involved in biological processes like Protein Modification by Small Protein Conjugation or Removal,

Proteolysis, and Regulation of Protein Modification Processes (Fig. 2G).

Construction and validation of a ubiquitination-related pathway gene signature for prognostic prediction in colorectal cancer

Subsequently, we assessed the prognostic significance of these 307 differentially expressed ubiquitination-related genes in colorectal cancer patients. Survival analysis revealed that 24 of these genes were significantly associated with patient prognosis. Among them, high expression levels of 14 genes were significantly correlated with poor overall survival, whereas low expression levels of the remaining 10 genes were also linked to unfavorable outcomes (Fig. 3A).

To develop a robust prognostic model based on ubiquitination-related genes, we performed LASSO regression analysis on these 24 prognostically significant genes. Through tenfold cross-validation, we identified the optimal lambda (λ) value that minimized the model's prediction error. At the optimal λ of 0.01, LASSO regression selected 14 genes as prognostic biomarkers (Fig. 3B, C). These 14 genes included BCL10 (B-cell CLL/lymphoma 10), HSPA1A (Heat Shock Protein Family A Member 1A), ASB10 (Ankyrin Repeat and SOCS Box Containing 10), FBXL5 (F-box and Leucine-Rich Repeat Protein 5), ADGRB1 (Adhesion G Protein-Coupled Receptor B1), RNF208 (Ring Finger Protein 208), H2AC6 (H2A Clustered Histone 6), USP26 (Ubiquitin Specific Peptidase 26), RBCK1 (RanBP-Type and C3HC4-Type Zinc Finger Containing 1), H2AC13 (H2A Clustered Histone 13), NTRK2 (Neurotrophic Receptor Tyrosine Kinase 2), FBXO15 (F-box Protein 15), AXIN2 (Axin 2), and CCNA1 (Cyclin A1). We calculated a risk score for each patient based on the expression levels of these genes using the following formula: Ubiquitination-Related Pathway Gene Signature (URPGS) = (− 0.399 × expression of BCL10) + (0.122 × expression of HSPA1A) + (0.072 × expression of ASB10) + (− 0.372 × expression of FBXL5) + (0.062 × expression of ADGRB1) + (0.027 × expression of RNF208) + (0.393 × expression of H2AC6) + (− 0.014 × expression of USP26) + (0.090 × expression of RBCK1) + (− 0.069 × expression of H2AC13) + (0.008 × expression of NTRK2) + (0.033 × expression of FBXO15) + (− 0.182 × expression of AXIN2) + (0.026 × expression of CCNA1).

The URPGS values, survival times, survival statuses, and expression profiles of the 14 genes for colorectal cancer patients are presented in Fig. 3D. Kaplan–Meier survival analysis demonstrated that patients in the URPGS-High subtype had significantly shorter overall survival compared to those in the URPGS-Low subtype (Fig. 3E). Time-dependent Receiver Operating Characteristic (ROC) curve analysis indicated that the risk score had good predictive accuracy for 1-year, 3-year, and 5-year prognosis, with Area Under the Curve (AUC) values of 0.77, 0.74, and 0.76, respectively (Fig. 3F). To further assess the robustness of the risk score model, we stratified the ccRCC population based on age, gender, stage, and MSS. After stratification of gender = female (Supplementary Fig. 1A), gender = male (Supplementary Fig. 1B), age ≤ 60 (Supplementary Fig. 1C), age > 60 (Supplementary Fig. 1D), stage = I and II (Supplementary Fig. 1E), stage = II and lV (Supplementary Fig. 1F) and MSS (Supplementary Fig. 1G). These results further confirmed the relatively good stratification ability of the prognostic model.

To validate the predictive capability of this model, we tested it on an independent validation cohort from the GSE87211 cohort. The results showed that the model exhibited strong predictive performance in the validation cohort as well. Patients in the URPGS-High subtype had significantly shorter overall survival and disease-free survival than those in the URPGS-Low subtype (Fig. 3G, H). These findings underscore the potential utility of URPGS as a prognostic tool for colorectal cancer, providing a basis for personalized risk assessment and aiding in clinical decision-making.

Correlation analysis between URPGS and clinical characteristics of colorectal cancer patients

Following the development of the URPGS, we proceeded to investigate its association with clinical characteristics in colorectal cancer patients. Our study found no significant difference in URPGS values between male and female patients (Fig. 4A). Likewise, URPGS values did not significantly differ between patients with Stage T3 and T4 tumors and those with Stage T1 and T2 tumors (Fig. 4B), nor between individuals without distant metastasis (Stage M0) and those with distant metastasis (Stage M1) (Fig. 4C). Conversely, patients with lymph node involvement (Stage N1 and N2) displayed markedly higher URPGS values compared to those without lymph node metastasis (Stage N0) (Fig. 4D). Additionally, those in advanced stages (Stage III and IV) had significantly elevated URPGS values compared to patients in early stages (Stage I and II) (Fig. 4E). Moreover, patients who experienced tumor recurrence exhibited significantly higher URPGS values than those without recurrence (Fig. 4F). These findings imply that an elevated URPGS correlates with lymph node metastasis, advanced disease stage, and recurrence, underscoring its potential as a prognostic biomarker in colorectal cancer.

Furthermore, we performed a comparative analysis of gene mutation profiles between the URPGS-Low and URPGS-High subtypes. In the URPGS-Low subtype, the top ten genes with the highest mutation rates were APC (Adenomatous Polyposis Coli), TTN (Titin), TP53 (Tumor Protein P53), KRAS (KRAS Proto-Oncogene,

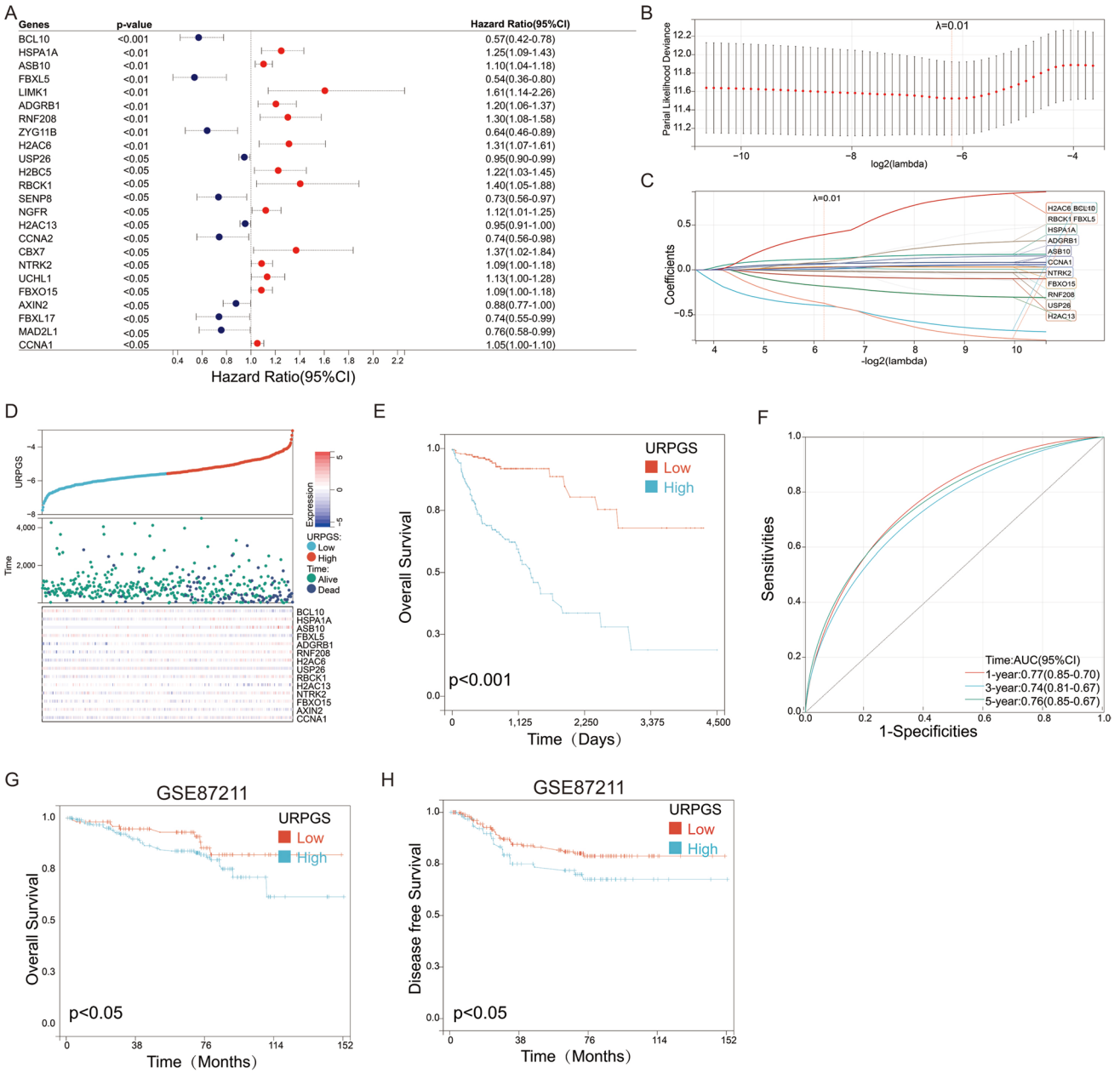

Fig. 3 Construction and validation of a URPGS for prognostic prediction in colorectal cancer. **A** Forest plot showing the hazard ratios and p-values of 24 ubiquitination-related genes significantly associated with patient prognosis. **B** LASSO regression analysis identifying the optimal lambda (λ) value for model selection. **C** Coefficient profiles of the 14 genes selected as prognostic biomarkers at the optimal λ of 0.01. **D** Distribution of URPGS values, survival times, survival statuses, and expression profiles of the 14 genes in colorectal cancer patients. **E** Kaplan–Meier survival analysis comparing overall survival between URPGS-High and URPGS-Low subtypes. **F** Time-dependent ROC curve analysis showing predictive accuracy for 1-year, 3-year, and 5-year prognosis. **G** and **H** Validation of the prognostic model in the GSE87211 cohort, demonstrating overall survival (**G**) and disease-free survival (**H**) differences between URPGS-High and URPGS-Low subtypes. The grouping of URPGS-Low and URPGS-High is established based on the optimal threshold. Statistical analysis was performed using the log-rank test to assess differences in survival outcomes

GTPase), PIK3CA (Phosphatidylinositol-4,5-Bisphosphate 3-Kinase Catalytic Subunit Alpha), SYNE1 (Spectrin Repeat Containing Nuclear Envelope Protein 1), MUC16 (Mucin 16), FAT4 (FAT Atypical Cadherin 4), DNAH5 (Dynein Axonemal Heavy Chain 5), and ZFHX4 (Zinc Finger Homeobox 4) (Fig. 4G). In the URPGS-High subtype, the top ten mutated genes were APC, TP53, TTN, KRAS, MUC16, SYNE1, RYR2 (Ryanodine Receptor 2), PIK3CA, OBSCN (Obscurin, Cytoskeletal Calmodulin and Titin-Interacting RhoGEF), and FAT4

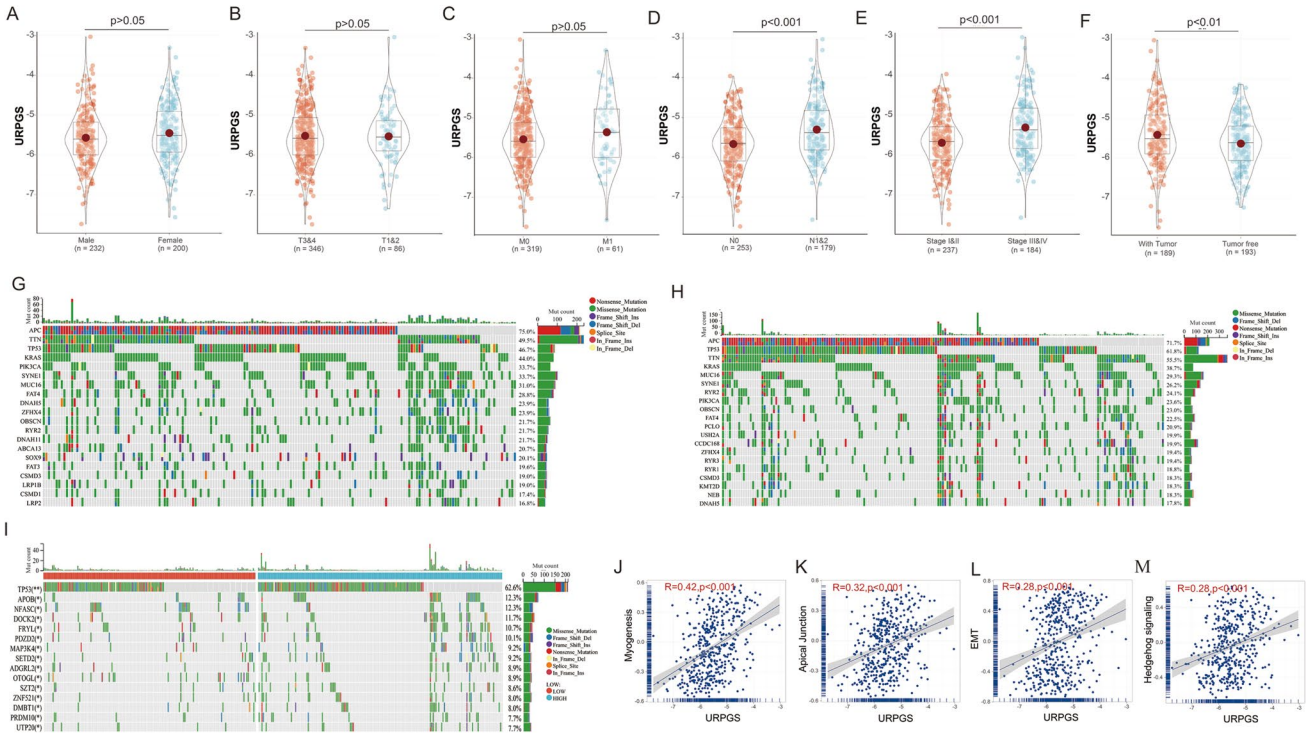

Fig. 4 Correlation analysis between URPGS and clinical characteristics of colorectal cancer patients. **A** Violin plot showing no significant difference in URPGS values between male and female patients. **B** Comparison of URPGS values between patients with Stage T3 and T4 and Stage T1 and T2 tumors. **C** URPGS values in patients without distant metastasis (Stage M0) versus those with distant metastasis (Stage M1). **D** Significantly higher URPGS values in patients with lymph node involvement (Stage N1 and N2) compared to those without (Stage N0). **E** Elevated URPGS values in Stage III and IV versus Stage I and II. **F** Higher URPGS values in patients with tumor recurrence compared to those without recurrence. **G** and **H** Mutation profiles of the genes in URPGS-Low (**G**) and URPGS-High (**H**) subtypes. **I** Differential mutation analysis between URPGS subtypes. **J**–**M** GSVA showing pathways positively correlated with URPGS: Myogenesis (**J**), Apical Junction (**K**), EMT (**L**), and Hedgehog Signaling (**M**)

(Fig. 4H). Subsequent differential mutation analysis between the two subtypes indicated that the URPGS-High subtype had a significantly higher mutation rate of TP53 (Fig. 4I). Given the pivotal role of TP53 mutations in cancer progression, this finding highlights the potential linkage between high URPGS values and more aggressive tumor biology.

Next, we conducted Gene Set Variation Analysis (GSVA) to identify signaling pathways associated with URPGS. The top four pathways positively correlated with URPGS were Myogenesis (R = 0.42), Apical Junction (R = 0.32), Epithelial-Mesenchymal Transition (EMT) (R = 0.28), and Hedgehog Signaling (R = 0.28) (Fig. 4J–M). These pathways are recognized for their critical roles in tumor development and metastasis, suggesting that URPGS may influence colorectal cancer progression via these signaling mechanisms.

Immune infiltration profiling and single-cell RNA sequencing analysis reveal distinct immune microenvironments and cellular heterogeneity in URPGS subtypes

To further elucidate the characteristics of the tumor immune microenvironment and cellular heterogeneity associated with URPGS subtypes, we conducted comprehensive immune infiltration analyses and single-cell RNA sequencing (scRNA-seq) analyses. Understanding the immune landscape and cellular composition of tumors is crucial for unraveling the mechanisms underlying tumor progression and for identifying potential therapeutic targets.

Firstly, we utilized the ESTIMATE and CIBERSORT algorithms to assess immune and stromal scores, as well as the proportions of various immune cell types in the URPGS-Low and URPGS-High subtypes. The ESTIMATE algorithm provides an estimation of the tumor microenvironment by calculating immune scores, stromal scores, and ESTIMATE scores. Our ESTIMATE analysis revealed that the URPGS-High subtype exhibited a significantly

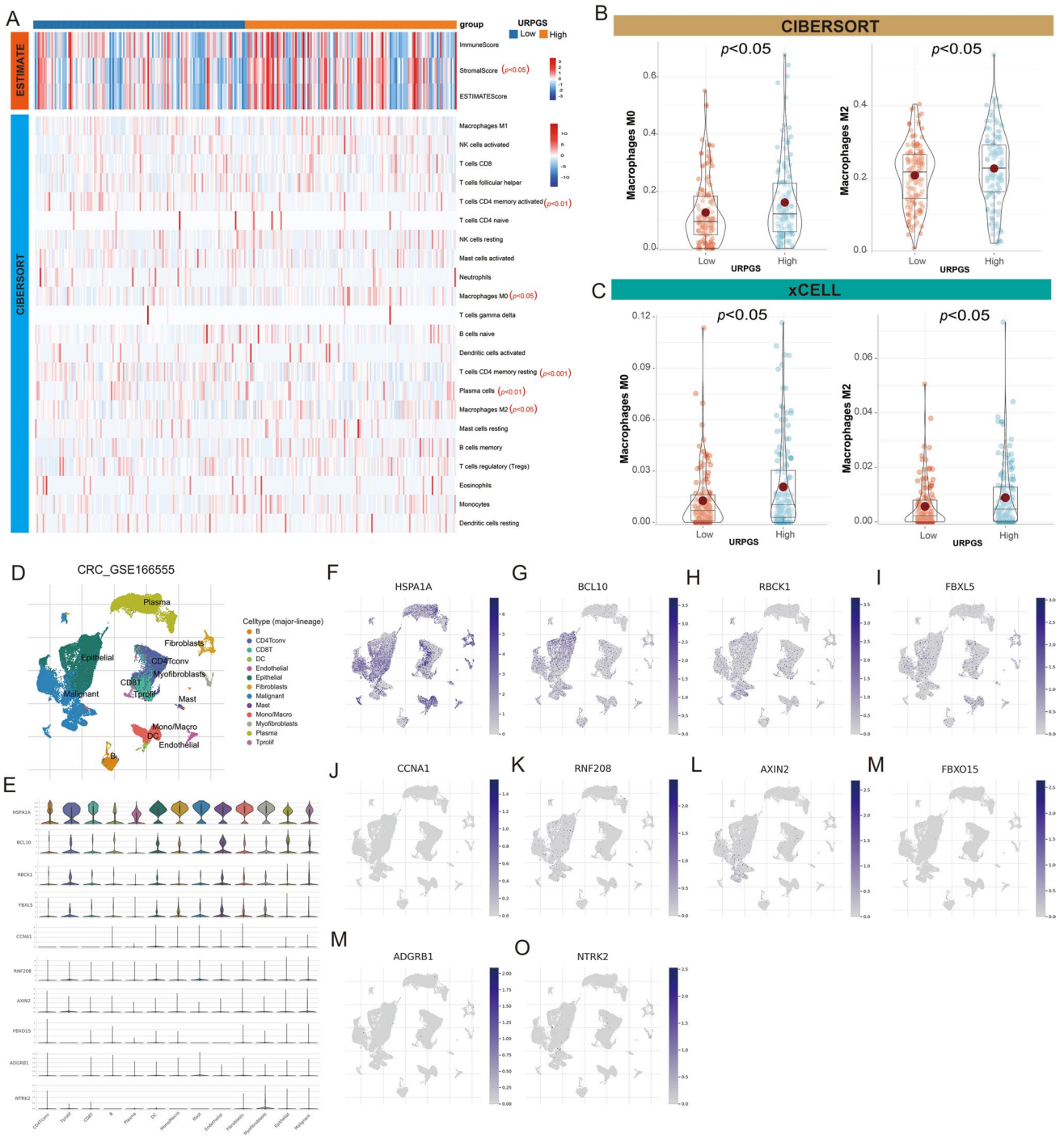

Fig. 5 Immune infiltration profiling and single-cell RNA sequencing analysis reveal distinct immune microenvironments and cellular heterogeneity in URPGS subtypes. **A** ESTIMATE analysis comparing stromal scores between URPGS-Low and URPGS-High subtypes, alongside CIBERSORT analysis of 22 immune cell types in these subtypes based on TCGA cohort. **B** CIBERSORT and **C** XCELL analyze the infiltration differences of M0 and M2 macrophages between the USPGS-Low and USPGS-High subtypes based on TCGA cohort. **D** Single-cell RNA sequencing analysis of the GSE166555 dataset. **E** Expression levels of URPGS model genes across various cell subtypes. **F–O** Expression of HSPA1A (**F**), BCL10 (**G**), RBCK1 (**H**), FBXL5 (**I**), CCNA1 (**J**), RNF208 (**K**), AXIN2 (**L**), FBXO15 (**M**), ADGRB1 (**N**), and NTRK2 (**O**) across different cell subtypes

higher stromal score compared to the URPGS-Low subtype (Fig. 5A), indicating a greater presence of stromal components in these tumors. However, there were no significant differences in the immune scores or the overall ESTIMATE scores between the two subtypes, suggesting that the total immune cell infiltration was similar.

To gain deeper insights into the specific immune cell populations contributing to the immune microenvironment, we performed CIBERSORT analysis to quantify the proportions of 22 immune cell types in each subtype. The results showed that, compared with the URPGS-Low subtype, the URPGS-High subtype had significantly higher infiltration of M0 and M2 macrophages, which are often associated with tumor-promoting and immunosuppressive functions (Fig. 5A, B). In contrast, the URPGS-High subtype exhibited lower infiltration of activated and resting CD4 memory T cells, as well as plasma cells, which play critical roles in antitumor immunity. To validate these findings, we conducted an XCELL analysis, which further corroborated the results from the CIBERSORT analysis. Consistently, the URPGS-High subtype showed increased infiltration of M0 and M2 macrophages compared to the URPGS-Low subtype (Fig. 5C). These results suggest that the URPGS-High tumors may foster an immunosuppressive microenvironment, contributing to tumor progression and poor prognosis.

Subsequently, to explore the cellular heterogeneity and gene expression patterns at the single-cell level, we analyzed the GSE166555 colorectal cancer single-cell RNA sequencing dataset. We examined the expression levels of genes included in the URPGS model across different cell subtypes within the tumor microenvironment (Fig. 5D–O). The analysis revealed that HSPA1A, BCL10, RBCK1, and FBXL5 were highly expressed across multiple cell subtypes, including B cells, CD8 T cells, endothelial cells, fibroblasts, malignant cells, monocytes/macrophages, myofibroblasts, and plasma cells. This widespread expression suggests that these genes may play pivotal roles in various cellular processes within the tumor microenvironment. In contrast, the other genes in the URPGS model exhibited weaker expression across the different cell subtypes.

These findings provide valuable insights into the distinct immune landscapes and cellular compositions of URPGS subtypes in colorectal cancer. The enrichment of immunosuppressive macrophages and the differential expression patterns of URPGS-related genes may contribute to the aggressiveness and poor prognosis associated with the URPGS-High subtype. Understanding these differences at both the bulk and single-cell levels may inform the development of targeted therapies aimed at modulating the tumor microenvironment to improve patient outcomes.

URPGS predicts the prognosis of colorectal cancer patients post-chemotherapy

Chemotherapy is a mainstay treatment for colorectal cancer, yet patient responses can vary widely owing to tumor heterogeneity. Identifying reliable prognostic biomarkers is essential for predicting treatment outcomes and guiding personalized therapy. Our earlier analyses highlighted the significant prognostic value of URPGS in colorectal cancer patients, prompting us to explore whether URPGS could also predict patient outcomes following chemotherapy.

Thus, we examined the relationship between URPGS and post-chemotherapy prognosis in colorectal cancer patients. In the TCGA cohort, among those who received chemotherapy, patients in the URPGS-High subtype experienced significantly shorter overall survival compared to those in the URPGS-Low subtype (Fig. 6A). Similarly, in the GSE17536 cohort, patients in the URPGS-High subtype showed markedly poorer overall survival than those in the URPGS-Low subtype following chemotherapy (Fig. 6B). These consistent findings across independent cohorts indicate that URPGS is a robust predictor of post-chemotherapy prognosis in colorectal cancer patients and could serve as a valuable tool for identifying patients at higher risk of poor outcomes despite undergoing chemotherapy.

Development of a nomogram for predicting overall survival

To provide personalized risk assessments and improve the predictive accuracy for patient outcomes, we further developed a nomogram by integrating the URPGS score with clinical variables such as gender and tumor staging parameters (T, N, and M stages). In this nomogram, each variable was assigned a specific point value based on its relative contribution to overall survival, and the total points were calculated by summing these values. This total score was then used to estimate the 1-year, 3-year, and 5-year overall survival probabilities for individual patients, offering a tailored risk evaluation (Fig. 7A). The Kaplan–Meier survival curves stratified by the total nomogram score demonstrated that patients with higher total points had significantly poorer overall survival compared to those with lower total points (Fig. 7B). This significant difference indicates the nomogram's efficacy in effectively distinguishing between high-risk and low-risk patient groups.

Additionally, we evaluated the predictive accuracy of the nomogram using ROC curves at 1-year, 3-year, and 5-year time points. The AUC values were 0.77 for 1-year, 0.74 for 3-year, and 0.74 for 5-year survival predictions (Fig. 7C). These AUC values suggest that the nomogram has good discriminative ability and reliably predicts patient survival over time.

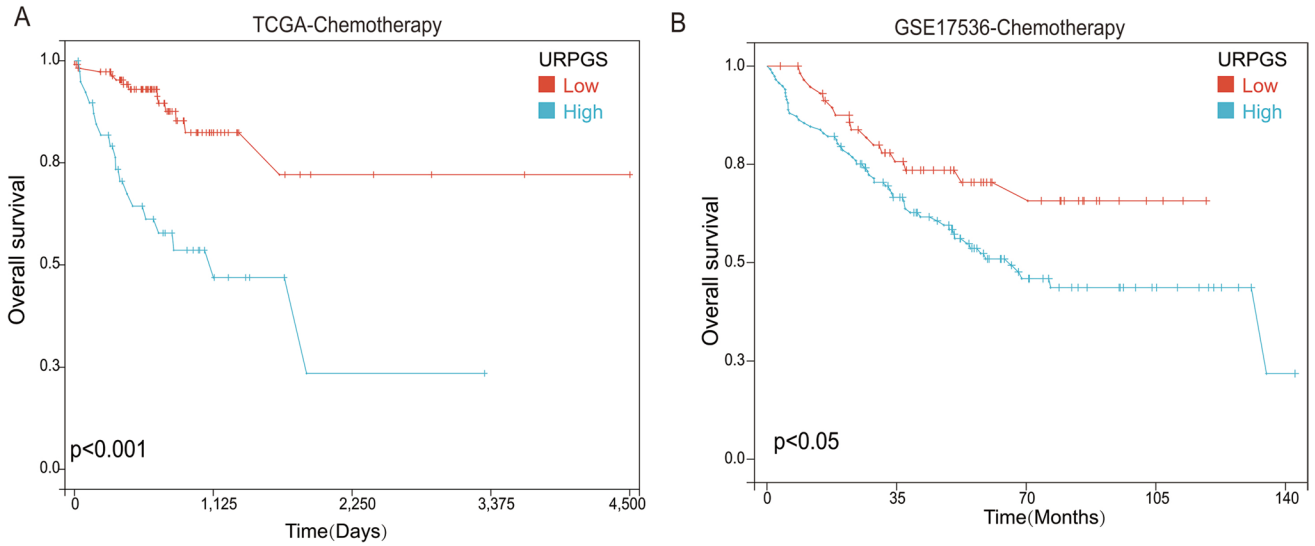

Fig. 6 URPGS as a predictor of post-chemotherapy prognosis in colorectal cancer patients. **A** Kaplan–Meier survival analysis of colorectal cancer patients from the TCGA cohort who underwent chemotherapy, showing significantly shorter overall survival for patients in the URPGS-High subtype compared to the URPGS-Low subtype. **B** Kaplan–Meier survival analysis of the GSE17536 cohort, confirming poorer overall survival in the URPGS-High subtype compared to the URPGS-Low subtype following chemotherapy. The grouping of URPGS-Low and URPGS-High is established based on the optimal threshold. Statistical analysis was performed using the log-rank test to assess differences in survival outcomes

Overall, the nomogram that integrates the URPGS score with clinical variables provides a valuable tool for individualized risk stratification and prognostic assessment in colorectal cancer patients. It may assist clinicians in making informed decisions regarding patient management and follow-up strategies, ultimately contributing to personalized medicine approaches in oncology.

Application of machine learning models and identification of HSPA1A as a key gene

To further enhance our understanding and improve the classification of colorectal cancer tissues versus adjacent normal tissues, we employed nine different machine learning models: XGBoost, Logistic Regression, LightGBM, Random Forest, AdaBoost, Decision Tree, Gradient Boosting Decision Tree (GBDT), Gaussian Naive Bayes (GNB), and Complement Naive Bayes (CNB). These models were utilized to perform classification tasks based on the expression profiles of 14 URPGS.

Among these models, the Random Forest classifier demonstrated relatively superior stability and performance in both the training and validation datasets (Fig. 8A–C). In the Random Forest model, the gene HSPA1A had the highest feature importance weight (Fig. 8D), suggesting its pivotal role in distinguishing colorectal cancer tissues from normal tissues. Consequently, we selected HSPA1A for further in-depth analysis.

Considering HSPA1A's significant role in our Random Forest model, we aimed to investigate its potential prognostic value in colorectal cancer. We conducted survival analyses using GSE17536, GSE17537, GSE28722, GSE29621, GSE39582, and TCGA cohorts. The results consistently indicated that patients with high HSPA1A expression had significantly poorer overall survival compared to those with low expression levels (Fig. 8E–J). Similarly, progression-free survival analyses based on GSE17536, GSE28722, GSE29621, GSE39582, GSE87211, and TCGA cohorts revealed that elevated HSPA1A expression was associated with worse clinical outcomes (Fig. 8K–P). Furthermore, disease-specific survival analyses using GSE17537, GSE87211, and TCGA cohorts showed that high HSPA1A expression correlated with reduced survival rates (Fig. 8Q–S). In addition, we assessed disease-free survival in patients stratified by HSPA1A expression using GSE143985, GSE161158, and TCGA cohorts. Consistent with our previous observations, patients with high HSPA1A expression exhibited significantly worse disease-free survival than those with low expression levels (Fig. 8T–V). These findings underscore the potential of HSPA1A as a prognostic biomarker in colorectal cancer.

Functional analysis of HSPA1A in colorectal cancer cells in vitro and in vivo

To further investigate the impact of HSPA1A on the proliferation and metastatic potential of colorectal cancer cells

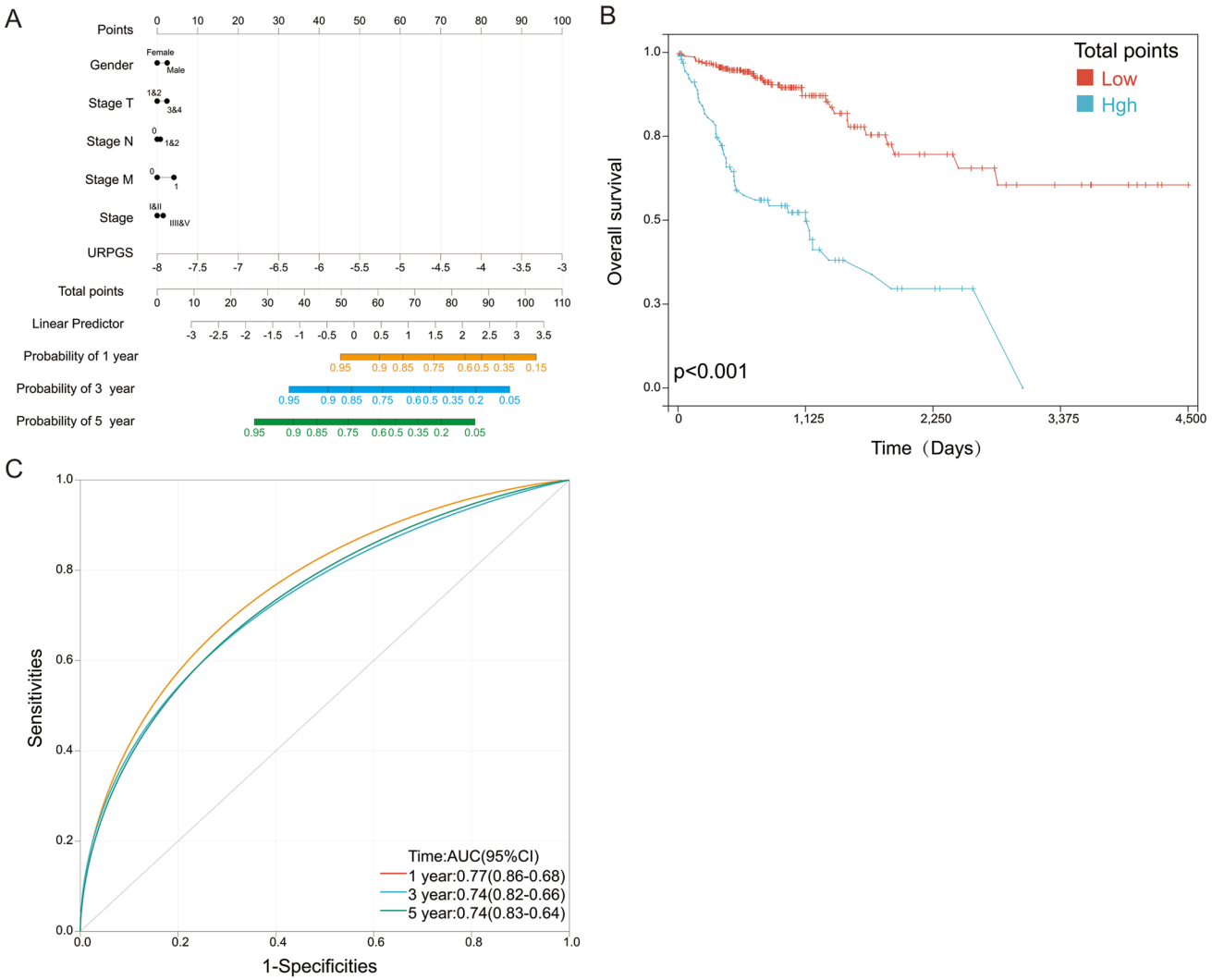

Fig. 7 Development of a Nomogram for predicting Overall Survival in colorectal cancer patients. **A** Nomogram integrating URPGS score with clinical variables (gender, T, N, and M stages) to estimate 1-year, 3-year, and 5-year overall survival probabilities. Each variable is assigned a point value, and the total score provides a personalized risk assessment. **B** Kaplan–Meier survival curves stratified by total nomogram score. **C** ROC curves evaluating the predictive accuracy of the nomogram at 1-year, 3-year, and 5-year intervals. The grouping of Total point-Low and Total point-High is established based on the optimal threshold. Statistical analysis was performed using the log-rank test to assess differences in survival outcomes

both in vitro and in vivo, we conducted a series of experiments using HCT116 and DLD-1 cell lines. Our objective was to elucidate how knockdown of HSPA1A influences the malignant behaviors of these cells.

In HCT116 cells, knockdown HSPA1A expression significantly inhibited their proliferation, migration, and invasion abilities (Fig. 9A–D). In DLD-1 cells, similar to HCT116 cells, HSPA1A knockdown significantly inhibited their proliferation, migration, and invasion abilities (Fig. 9E–H), further supporting the promoter role of HSPA1A in the progression of colorectal cancer.

To validate our in vitro findings in an in vivo context, we established a zebrafish xenograft model of HCT-116 cells to assess tumor proliferation and metastasis. At 2 h post-transplantation (hpt), there was no significant difference in fluorescence intensity between the HSPA1A knockdown group (HSPA1A-shRNA) and the negative control group (NC), indicating similar initial tumor cell distribution. However, by 48 h post-transplantation, the fluorescence intensity in the HSPA1A knockdown group was significantly reduced compared to the NC group (Fig. 10A), demonstrating that HSPA1A knockdown effectively inhibited tumor cell proliferation within the zebrafish model. In addition to proliferation, we also analyzed the metastatic potential of HCT-116 cells using tail fluorescence imaging (Fig. 10B). At 2 h post-transplantation, there was no

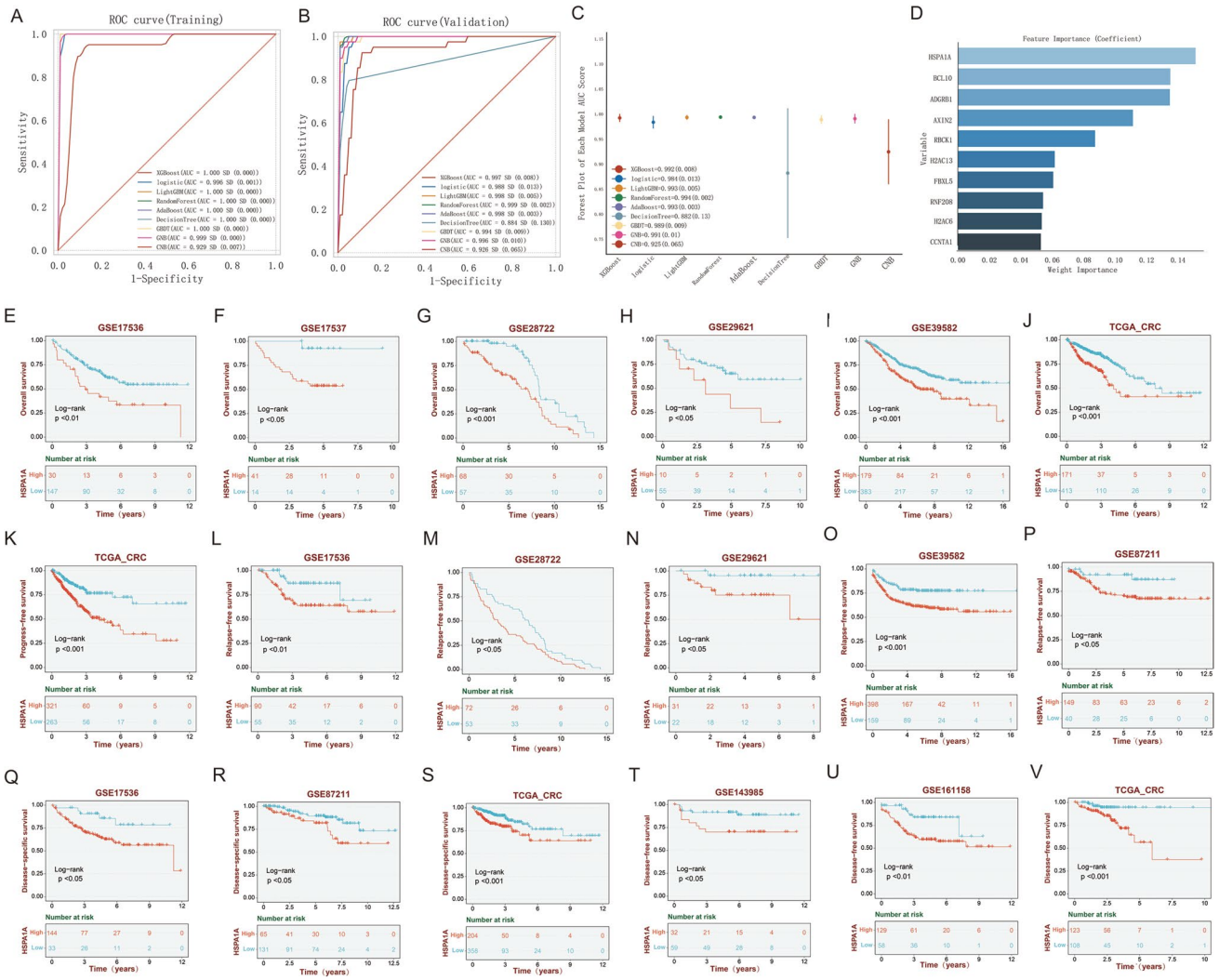

Fig. 8 Application of machine learning models and identification of HSPA1A as a key gene in colorectal cancer. **A** and **B** ROC curves for training (**A**) and validation (**B**) datasets using nine machine learning models. **C** Comparison of model AUC scores. **D** Feature importance in the Random Forest model, with HSPA1A showing the highest weight. **E–J** Overall survival analyses in cohorts GSE17536 (**E**), GSE17537 (**F**), GSE28722 (**G**), GSE29621 (**H**), GSE39582 (**I**), and TCGA (**J**), indicating poorer survival for patients with high HSPA1A expression. **K** and **P** Progression-free survival analyses in TCGA (**K**), GSE17536 (**L**), GSE28722 (**M**), GSE29621 (**N**), GSE39582 (**O**), and GSE87211 (**P**), showing worse outcomes with elevated HSPA1A expression. **Q–S** Disease-specific survival analyses in GSE17537 (**Q**), GSE87211 (**R**), and TCGA (**S**), correlating high HSPA1A expression with reduced survival rates. **T–V** Disease-free survival analyses in GSE143985 (**T**), GSE161158 (**U**), and TCGA (**V**), confirming significantly worse survival for patients with high HSPA1A expression. The grouping of HSPA1A-Low and HSPA1A-High is established based on the optimal threshold. Statistical analysis was performed using the log-rank test to assess differences in survival outcomes

significant difference in tail fluorescence area between the HSPA1A knockdown group and the NC group. However, by 24 h, the HSPA1A knockdown group exhibited a significant reduction in tail fluorescence area compared to the NC group, suggesting that knockdown of HSPA1A effectively curtailed tumor cell migration. This in vivo evidence corroborates our in vitro results and underscores the potential of HSPA1A as a therapeutic target for inhibiting colorectal cancer progression.

Discussion

The ubiquitination pathway is a crucial post-translational modification process that impacts protein stability and function, influencing cellular processes like apoptosis and DNA repair. In colorectal cancer (CRC), dysregulation of ubiquitination-related pathways can provide insights into tumorigenesis and identify therapeutic targets.

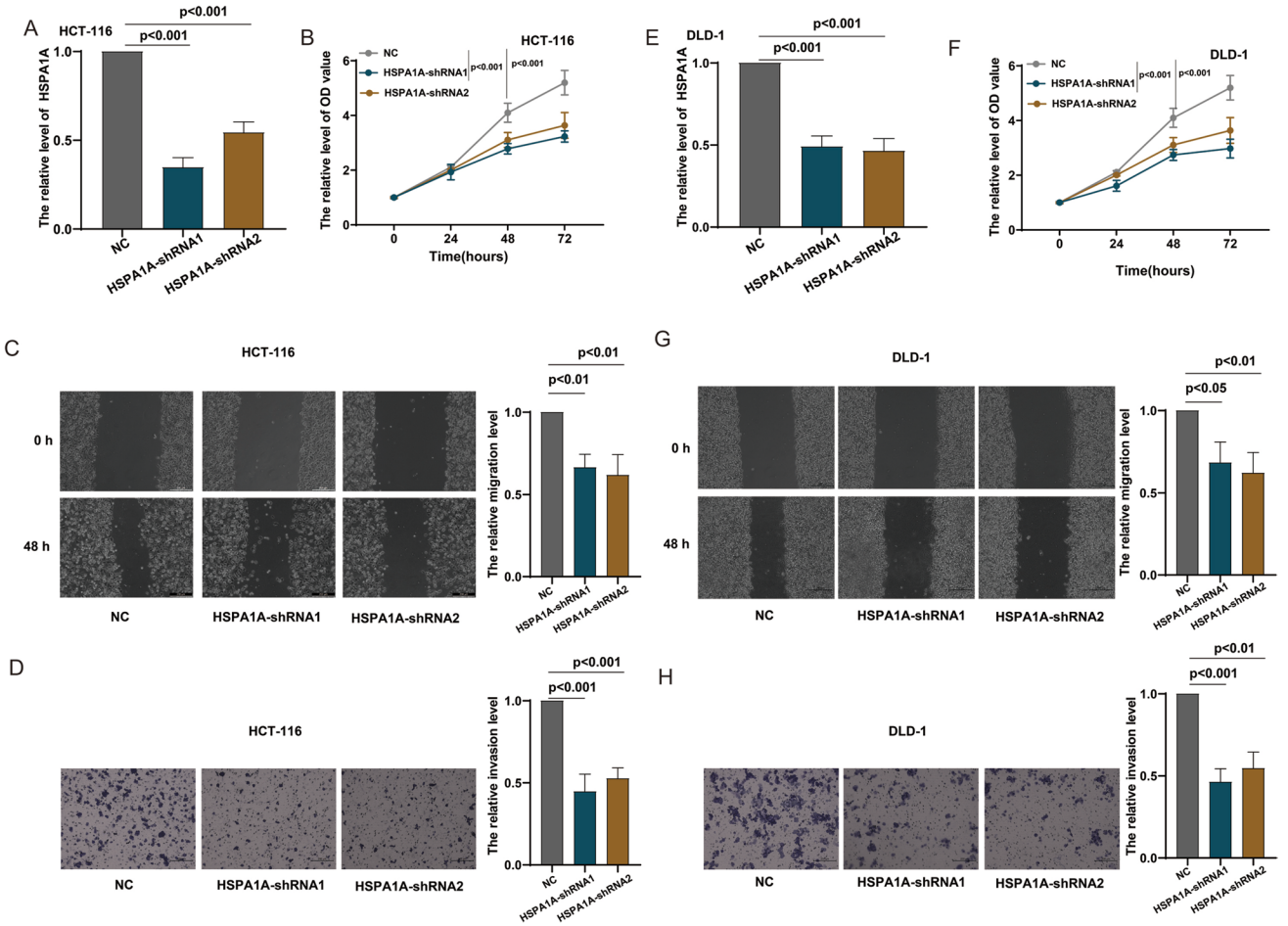

Fig. 9 Knockdown of HSPA1A inhibits proliferation and metastasis of colorectal cancer cells in vitro. **A** RT-PCR analysis of HSPA1A gene expression after HSPA1A knockdown in HCT-116 cells. **B** CCK8 assay to assess changes in proliferation capacity after HSPA1A knockdown in HCT-116 cells. **C** Scratch assay to evaluate changes in migration ability after HSPA1A knockdown in HCT-116 cells. **D** Transwell assay to examine changes in invasion capacity after HSPA1A knockdown in HCT-116 cells. **E** RT-PCR analysis of HSPA1A gene expression after HSPA1A knockdown in DLD-1 cells. **F** CCK8 assay to assess changes in proliferation capacity after HSPA1A knockdown in DLD-1 cells. **G** Scratch assay to evaluate changes in migration ability after HSPA1A knockdown in DLD-1 cells. **H** Transwell assay to examine changes in invasion capacity after HSPA1A knockdown in DLD-1 cells

Our study assessed the expression profiles of 1,006 genes across 46 ubiquitination-related pathways in CRC tissues, identifying 144 upregulated and 163 downregulated genes. These alterations highlight significant changes in the ubiquitination landscape, underscoring the potential of these genes as diagnostic biomarkers.

A subset of 24 genes associated with patient prognosis formed the URPGS, demonstrating strong predictive capabilities in independent cohorts. Higher URPGS values correlated with poor outcomes and advanced disease stages, indicating its utility in patient stratification. Additionally, the URPGS-High subtype exhibited a higher TP53 mutation rate, suggesting a more aggressive cancer phenotype. Our GSVA analysis linked URPGS with critical pathways, such as EMT and Hedgehog signaling, known for their roles in cancer progression. Overall, these findings support the potential of URPGS for prognostication and therapeutic strategies in CRC.

Our immune infiltration profiling and single-cell RNA sequencing analyses provided deeper insights into the tumor microenvironment and cellular heterogeneity associated with URPGS subtypes. The URPGS-High subtype exhibited higher infiltration of immunosuppressive M0 and M2 macrophages, along with lower levels of activated CD4 memory T cells and plasma cells. This immunosuppressive microenvironment may contribute to tumor progression and resistance to therapy [10–12]. At the single-cell level, key genes in the URPGS model, such as HSPA1A, BCL10, RBCK1, and FBXL5, were highly expressed across multiple cell types within the tumor microenvironment, suggesting their broad functional roles.

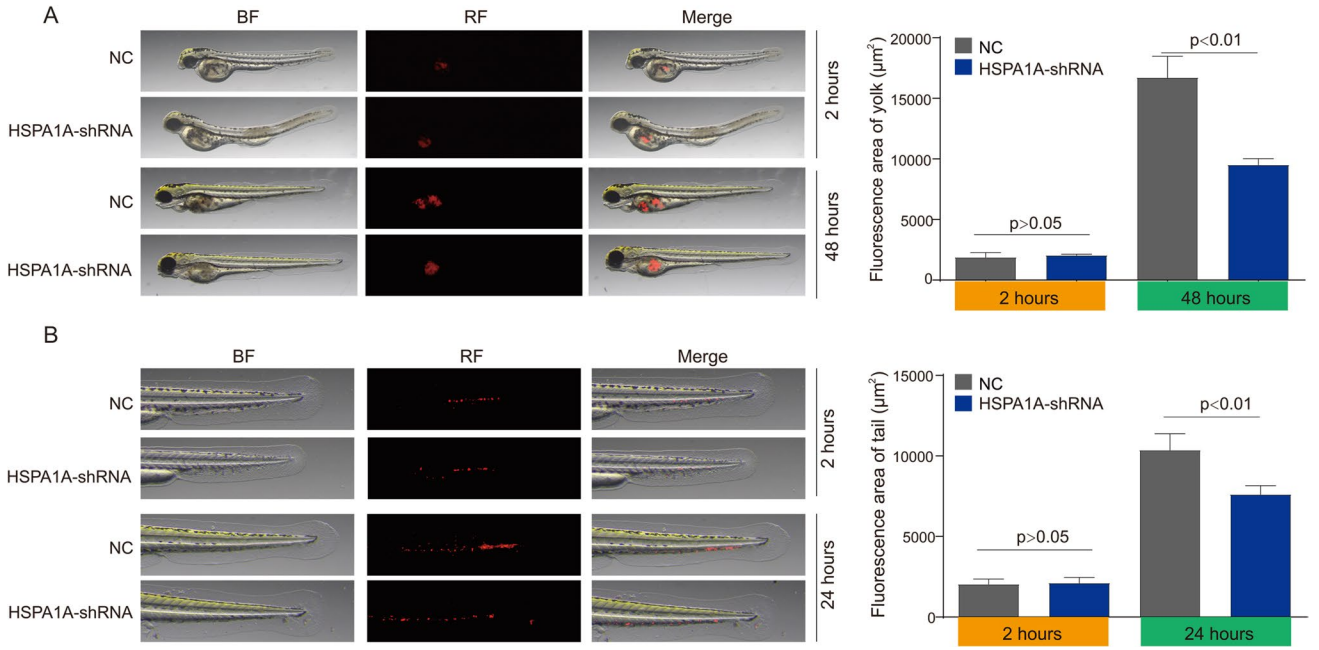

Fig. 10 Knockdown of HSPA1A inhibits proliferation and metastasis of colorectal cancer cells in vivo. **A** and **B** Effects of HSPA1A knockdown on **A** proliferation and **B** metastasis of HCT-116 cells in zebrafish models

The exploration of URPGS as a predictor of chemotherapy outcomes further emphasizes its clinical utility. The consistent findings across TCGA and GSE17536 cohorts demonstrate its potential applicability in evaluating patient responses to chemotherapy, allowing for more personalized therapeutic strategies. Indeed, patients with high URPGS values exhibited poorer survival despite chemotherapy, indicating that URPGS could help identify patients who might benefit from alternative or adjunctive treatments. The development of a nomogram integrating URPGS with clinical parameters such as tumor stage further refines risk assessment models for colorectal cancer patients.

The URPGS model has significant potential clinical applications, particularly in guiding personalized treatment strategies and predicting chemotherapy responses in CRC patients. By stratifying patients into high-risk and low-risk groups based on their URPGS scores, clinicians can tailor treatment plans that are more aligned with the individual patient's prognosis. For instance, patients identified as high-risk may benefit from more aggressive treatment regimens, including combination therapies or novel targeted therapies, while low-risk patients might be suitable for less intensive treatment approaches. Moreover, the URPGS model can serve as a valuable tool for predicting chemotherapy responses. Our findings indicate that patients with high URPGS scores experienced poorer overall survival despite receiving chemotherapy. This suggests that the URPGS model could help identify patients who may not respond well to standard chemotherapy, allowing for the exploration of alternative therapeutic options or the incorporation of adjunctive treatments that could enhance efficacy.

Importantly, HSPA1A emerged as a significant gene within our study. Identified as the gene with the highest feature importance within the Random Forest model for distinguishing tumor tissues, HSPA1A showed a consistent correlation of high expression with poorer prognosis across various survival metrics, highlighting its potential as a critical biomarker and therapeutic target. HSPA1A, also known as HSP70, is a stress-inducible heat shock protein that functions as a molecular chaperone, assisting in protein folding and preventing aggregation of misfolded proteins [13–16]. It is involved in the ubiquitin–proteasome pathway through its interaction with proteins destined for degradation [17]. Specifically, HSPA1A facilitates the delivery of misfolded and damaged proteins to the ubiquitin–proteasome system, interacting with E3 ubiquitin ligases, thereby regulating protein homeostasis and turnover [18]. In a pan-cancer analysis, HSPA1A expression was generally associated with poor prognosis in tumors of the respiratory, digestive, urinary, and reproductive systems, while it was linked to a favorable prognosis in cholangiocarcinoma, pheochromocytoma, and paraganglioma [19]. The complex and sometimes conflicting roles of HSPA1A across different cancers underscore its potential as a universal biomarker and highlight the need for further investigation into its mechanistic contributions to tumor biology.

Our in vitro and in vivo functional studies affirmed the oncogenic role of HSPA1A, with its knockdown markedly

reducing colorectal cancer cell proliferation and metastasis. These results suggest that HSPA1A not only serves as a biomarker for prognosis but may also be directly involved in tumorigenesis through its role in the ubiquitination pathway. Targeting HSPA1A may provide a novel therapeutic strategy, as its knockdown has been shown to inhibit CRC cell proliferation, migration, and invasion in vitro, as well as tumor growth and metastasis in vivo. By modulating HSPA1A expression or function, it may be possible to enhance the effectiveness of existing treatments or develop new therapeutic approaches that specifically target the mechanisms underlying CRC progression.

Emerging research has increasingly illuminated the downstream signaling pathways modulated by HSPA1A. Compelling evidence demonstrates that HSPA1A overexpression can potently activate the Wnt/β-catenin signaling pathway [20]. Moreover, HSPA1A exhibits a remarkable ability to bind and stabilize p53 [21], effectively preventing its ubiquitination and subsequent degradation. This critical interaction empowers p53 to preserve its fundamental tumor suppressor functions, including cell cycle arrest and programmed cell death. Within the intricate ubiquitination machinery, HSPA1A engages with a diverse array of key proteins, with particular emphasis on E3 ubiquitin ligases and proteasomal components. These sophisticated interactions are instrumental in maintaining cellular protein homeostasis and orchestrating the precise degradation of misfolded proteins. By modulating E3 ligase activity, HSPA1A strategically influences the stability of various molecular substrates, ranging from oncogenes to tumor suppressor proteins, thereby significantly impacting colorectal cancer progression.

The functional role of HSPA1A in colorectal cancer presents a nuanced dichotomy, oscillating between its characterization as an oncogene and a stress-response protein. Traditionally perceived as a cellular protective mechanism against damage, its pronounced overexpression in colorectal cancer increasingly suggests a more complex oncogenic potential. Notably, elevated HSPA1A levels correlate strongly with poor prognosis and aggressive tumor behavior, implying its capacity to drive tumor growth and metastasis. This multifaceted functionality underscores the intricate nature of HSPA1A in colorectal cancer, simultaneously serving as a cellular stress guardian and a potential oncogenic facilitator.

Conclusion

In conclusion, our comprehensive analysis highlights the critical role of ubiquitination-related pathways in colorectal cancer progression and prognosis. The URPGS is a valuable prognostic tool that correlates with clinical characteristics and patient outcomes, including responses to chemotherapy. HSPA1A is identified as a key tumor promoter gene with significant potential as a prognostic biomarker and therapeutic target. These findings enhance our understanding of colorectal cancer biology and may contribute to the development of personalized therapeutic strategies aimed at improving patient outcomes.

Supplementary Information The online version contains supplementary material available at https://doi.org/10.1007/s12032-025-02662-z.

Acknowledgements N/A.

Author contributions X.G, T.Y, and X.Y carried out the bioinformatic analyses. Q.L and L.Z conducted the experiments. Q.W, and J.W supervised the work and wrote the manuscript. All authors reviewed the manuscript.

Funding This work was supported by Fujian University of Traditional Chinese Medicine (X2023022).

Data Availability No datasets were generated or analysed during the current study.

Declarations

Conflict of interest The authors declare no competing interests.

Consent to participate N/A.

Ethical approval N/A.

References

1. Biller LH, Schrag D. Diagnosis and treatment of metastatic colorectal cancer: a review. JAMA. 2021;325:669–85.
2. Patel SG, Karlitz JJ, Yen T, Lieu CH, Boland CR. The rising tide of early-onset colorectal cancer: a comprehensive review of epidemiology, clinical features, biology, risk factors, prevention, and early detection. Lancet Gastroenterol Hepatol. 2022;7:262–74.
3. Eng C, Jácome AA, Agarwal R, Hayat MH, Byndloss MX, Holowatyj AN, Bailey C, Lieu CH. A comprehensive framework for early-onset colorectal cancer research. Lancet Oncol. 2022;23:e116–28.
4. Yan H, Talty R, Johnson CH. Targeting ferroptosis to treat colorectal cancer. Trends Cell Biol. 2023;33:185–8.

5. Ashktorab H, Brim H. Colorectal cancer subtyping. Nature reviews. Cancer. 2022;22:68–9.
6. Smith JJ, Deane NG, Wu F, Merchant NB, Zhang B, Jiang A, Lu P, Johnson JC, Schmidt C, Bailey CE, Eschrich S, Kis C, Levy S, Washington MK, Heslin MJ, Coffey RJ, Yeatman TJ, Shyr Y, Beauchamp RD. Experimentally derived metastasis gene expression profile predicts recurrence and death in patients with colon cancer. Gastroenterology. 2010;138:958–68.
7. Hu Y, Gaedcke J, Emons G, Beissbarth T, Grade M, Jo P, Yeager M, Chanock SJ, Wolff H, Camps J, Ghadimi BM, Ried T. Colorectal cancer susceptibility loci as predictive markers of rectal cancer prognosis after surgery. Genes Chromosom Cancer. 2018;57:140–9.
8. Sun Y, Chen Y, Zhuang W, Fang S, Chen Q, Lian M, Lv C, Weng J, Wei R, Lin Y, Cai L, Wang Q. Gastric cancer peritoneal metastasis related signature predicts prognosis and sensitivity to immunotherapy in gastric cancer. J Cell Mol Med. 2023;27:3578–90.
9. Han Y, Wang Y, Dong X, Sun D, Liu Z, Yue J, Wang H, Li T, Wang C. TISCH2: expanded datasets and new tools for single-cell transcriptome analyses of the tumor microenvironment. Nucleic Acids Res. 2023;51:D1425–31.
10. Yunna C, Mengru H, Lei W, Weidong C. Macrophage M1/M2 polarization. Eur J Pharmacol. 2020;877: 173090.
11. Mantovani A, Sozzani S, Locati M, Allavena P, Sica A. Macrophage polarization: tumor-associated macrophages as a paradigm for polarized M2 mononuclear phagocytes. Trends Immunol. 2002;23:549–55.
12. Chen T, Cao Q, Wang Y, Harris DCH. M2 macrophages in kidney disease: biology, therapies, and perspectives. Kidney Int. 2019;95:760–73.
13. Wang WF, Yan L, Liu Z, Liu LX, Lin J, Liu ZY, Chen XP, Zhang W, Xu ZZ, Shi T, Li JM, Zhao YL, Meng G, Xia Y, Li JY, Zhu J. HSP70-Hrd1 axis precludes the oncorepressor potential of N-terminal misfolded Blimp-1s in lymphoma cells. Nat Commun. 2017;8:363.
14. Wu S, Pei Q, Ni W, Fu X, Zhang W, Song C, Peng Y, Guo Q, Dong J, Yao M. HSPA1A protects cells from thermal stress by impeding ESCRT-0-mediated autophagic flux in epidermal thermoresistance. J Invest Dermatol. 2021;141:48-58.e3.
15. He X, Guo X, Deng B, Kang J, Liu W, Zhang G, Wang Y, Yang Y, Kang X. HSPA1A ameliorated spinal cord injury in rats by inhibiting apoptosis to exert neuroprotective effects. Exp Neurol. 2023;361: 114301.
16. Vandova V, Vankova P, Durech M, Houser J, Kavan D, Man P, Muller P, Trcka F. HSPA1A conformational mutants reveal a conserved structural unit in Hsp70 proteins. Biochim Biophys Acta. 2020;1864: 129458.
17. Seo JH, Park JH, Lee EJ, Vo TT, Choi H, Kim JY, Jang JK, Wee HJ, Lee HS, Jang SH, Park ZY, Jeong J, Lee KJ, Seok SH, Park JY, Lee BJ, Lee MN, Oh GT, Kim KW. ARD1-mediated Hsp70 acetylation balances stress-induced protein refolding and degradation. Nat Commun. 2016;7:12882.
18. Mayer MP. Hsp70 chaperone dynamics and molecular mechanism. Trends Biochem Sci. 2013;38:507–14.
19. Yan LR, Shen SX, Wang A, Ding HX, Liu YN, Yuan Y, Xu Q. Comprehensive pan-cancer analysis of heat shock protein 110, 90, 70, and 60 families. Front Mol Biosci. 2021;8: 726244.
20. Zhang W, Xue D, Yin H, Wang S, Li C, Chen E, Hu D, Tao Y, Yu J, Zheng Q, Gao X, Pan Z. Overexpression of HSPA1A enhances the osteogenic differentiation of bone marrow mesenchymal stem cells via activation of the Wnt/β-catenin signaling pathway. Sci Rep. 2016;6:27622.
21. Boysen M, Kityk R, Mayer MP. Hsp70- and Hsp90-mediated regulation of the conformation of p53 DNA binding domain and p53 cancer variants. Mol Cell. 2019;74:831-43.e4.